International Journal of Mechanical Engineering Science and Technology
ISSN: 3163-5040 (Online)

Vol. 1, No. 2 (2026) | Page 86– 95 | Received: 08 Agust 2026 Revised: 1 September 2026 Accepted: 26 September 2026

Development of Chitosan-Based Graphene Hydrogel for Efficient Solar Evaporation

Hooi Peng Lim[1*], Limi Chong[2], Ida Rosmanizan Abdullah[3]

[1] *Department of Mechanical Engineering, Politeknik Ibrahim Sultan, Pasir Gudang, Johor, Malaysia*
[2] *Department of Mechanical Engineering, Politeknik Kota Kinabalu, Kota Kinabalu, Sabah, Malaysia*
[3] *Department of Mechanical Engineering, Politeknik Kota Kinabalu, Kota Kinabalu, Sabah, Malaysia*

Corresponding author: Hooi Peng Lim, limhooipeng@pis.edu.my

A B S T R A C T

This study aims to evaluate the effectiveness of developing a chitosan-derived graphene hydrogel for a solar evaporation system. The hydrogel was prepared in two types, i.e. flat-surface and hemispherical-surface hydrogels. The system consisted of a chitosan-derived embedded graphene hydrogel, a cotton wipe, and a thermal insulator. The system was then tested using a solar simulator to investigate the effect of varying irradiation times from 1 to 12 hours. The morphology of the hydrogel was characterised using an inverted microscope before and after irradiation for 1 and 12 hours, respectively. The experimental test includes temperature distribution and water mass loss for the samples before and after irradiation for 1 and 12 hours. The resultant findings provide useful data on the evaporation system efficiency under the simulated conditions. It was reported that the hemispherical-surface hydrogel reached a lower temperature distribution of 52 °C than the flat-surface hydrogel at 57 °C. The water mass loss of the hemispherical-surface hydrogel is as low as -1.22 g, indicating a higher evaporation rate of 0.09205 kgm−2 h−1 than the flat-surface hydrogel of -1.48 g and 0.04568 kgm−2 h−1, respectively. This study reveals that a lower total water mass loss can occur alongside a higher evaporation rate when the surface area exposed to air is very small, as in a hemispherical-surface hydrogel.

K E Y W O R D S : Evaporation System; Hydrogel; Irradiation; Absorbent and Water; Mass Loss.

1. INTRODUCTION

A significant method of harnessing solar energy is through solar absorber technology, a solar-thermal system that effectively stores solar radiation using photothermal materials. Due to their greater light absorption and extremely effective thin-layer evaporation, coupled with minimal heat loss or transit, photothermal materials often have high solar energy conversion efficiency. For high-performance solar absorber systems, it is crucial to use photothermal materials with high light absorption, low thermal conductivity, and interpenetrated porous structures, such as carbon or graphene oxides. The most important challenge in photothermal materials is synthesising or fabricating super-absorbing materials that rapidly absorb solar energy. For this purpose, biodegradable materials such as starch, cellulose derivatives, and chitosan would be ideal in addition to photothermal materials. Chitosan outperforms other biodegradable materials due to its excellent biodegradability and biocompatibility. To date, limited studies have investigated the fabrication of a photothermal hydrogel using chitosan and graphene. Therefore, the purpose of this study is to synthesise an eco-friendly chitosan-derived graphene hydrogel for efficient solar absorption by examining the effects of flat- and hemispherical-surface hydrogels, based on morphological characterisation and surface temperature measurements under a solar simulator, on water mass loss. The objectives of the study include (1) to produce an eco-friendly evaporation system using chitosan-derived, graphene hydrogel for an efficient solar absorber, (2) to characterise the morphology of the chitosan-derived, graphene hydrogel, and (3) to investigate the effect of the irradiated solar simulator on the absorber temperature and water mass loss.

© 2026 The Authors. This work is licensed under a Creative Commons Attribution 4.0 International License

Chitosan, derived from chitin, which is abundant in arthropods, fungi, and microorganisms, has garnered significant interest in its biocompatibility, antimicrobial properties, and versatility. Despite production scalability and processing challenges, ongoing research underscores Chitosan's potential to address diverse societal and environmental needs while promoting sustainable practices across industries [1]. The abundantly available chitin, which is the precursor of chitosan, is well-known for its functionality in the exoskeletons of arthropods, fungi's cell walls, green algae and various microorganisms [1], [2]. Besides, chitin also has other properties, such as biocompatibility, biodegradability, and antimicrobial activity, and it can form films and gels. This makes them versatile in various applications. The effects of source and processing method on the morphology and physical characteristics of chitosan result in differences in molecular weight, degree of deacetylation, crystallinity, and polymer chain conformation. Chitosan exhibited an amorphous or semi-crystalline morphology, with fibrous or flake-like structures, and was white to off-white in colour. They are insoluble in water and exhibit neutral pH. But they become soluble under acidic conditions, likely due to protonation of their amino groups, and form polycationic chains [1]. The ability of chitosan to form gels, films and nanoparticles can be attributed to this solubility behaviour. The versatility of chitosan makes it useful in various applications. Based on the film-forming ability of chitosan and its capacity for adsorbing heavy metals, organic compounds, and other compatible materials, this study proposed embedding chitosan with graphene to produce a hydrogel. Figure 1 shows the morphology-based dressing of chitosan. Besides their versatile morphology characteristics, chitosan also possesses good mechanical stability. Previous studies have incorporated nanomaterials into chitosan to form nanocomposites, thereby enhancing properties. Other studies attempt to modify chitosan to fabricate a gel system that yields mechanically stable chitosan [3], [4], [5].

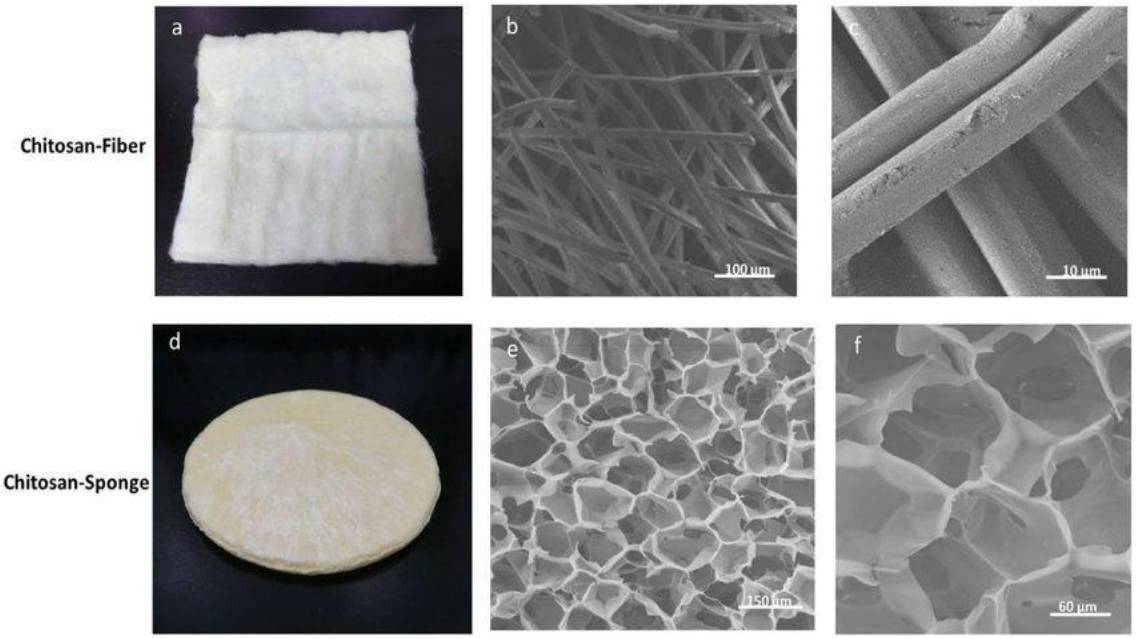


Figure 1. (a) Chitosan-fibre (CF) dressing; (b) Electron microscopic structure of CF dressing at 100× magnification; (c) Electron microscopic structure of CF dressing at 1000× magnification; (d) Chitosan-sponge (CS) dressing; (e) Electron microscopic structure of CS dressing at 100× magnification; (f) Electron microscopic structure of CS dressing at 250× magnification [6]

An advanced material derived from graphene, known as graphene hydrogel, was synthesised and is of increasing interest to researchers due to its extraordinary properties and versatility across various applications. The synergistic effects of combining graphene with hydrogels resulted in a graphene hydrogel with increased strength, conductivity, and biocompatibility [7], [8], [9], [10]. They are capable of producing a three-dimensional network structure, synthesised by reducing graphene oxide, yielding high porosity and surface area, making them suitable for energy storage and electronic applications. As research progresses, graphene hydrogel possesses unique morphological and physical properties that distinguish it from ordinary materials. Numerous studies reported that the morphology of the graphene hydrogel was porous and sponge-like, carrying a high surface area-to-volume ratio

© 2026 The Authors. This work is licensed under a Creative Commons Attribution 4.0 International License

[7], [8], [9], [10]. Efficient mass transport and interactions with sounding molecules were enhanced by this morphology, making the graphene hydrogel best suited for absorption, sensing, and catalysis. The graphene hydrogel also showed exceptional mechanical strength, flexibility, and electrical conductivity. Graphene oxides, known for their unique two-dimensional structure, contributed to increased mechanical strength and tensile strength of the hydrogel [3], [5], [10]. Graphene oxides often excel as fillers that enhance the hydrogel's mechanical properties when incorporated. They contain abundant oxygen-containing functional groups, which facilitate strong interactions with the polymer matrix, i.e., chitosan [3], [5], [10]. Compared with carbon nanoparticles, graphene oxides promote stronger crosslinking and stability within the hydrogel, thereby significantly improving its chemical compatibility. The hydrogel's adsorptive capacity and selectivity can be further improved by graphene's high specific surface area and electronegativity.

2. METHODOLOGY

The methodology for developing an eco-friendly evaporation system using a chitosan-derived/ graphene hydrogel for solar evaporation involved several steps. Chitosan and graphene were combined to form a hydrogel through cross-linking. The hydrogel was then shaped into two structures (namely, flat-surface hydrogel and hemispherical-surface hydrogel) for steam generation. In general, the hydrogel absorbed water from a heat source, such as sunlight or waste heat, and converted it into steam through evaporation. Steam could be collected and utilised for various applications, such as sterilisation or power generation. This approach offered a sustainable solution for steam generation, utilising renewable materials and minimising environmental impact. Figure 2 shows the fabrication process for producing the chitosan-derived/ graphene hydrogel. Firstly, 1 g of chitosan, a natural polymer derived from chitin, was dissolved in an appropriate solvent, i.e., 50 ml of acetic acid. Then, the chitosan and acetic acid solution was mixed with 4 g of graphene dissolved in 50 ml of distilled water, producing a graphene-derived chitosan solution that could increase water absorption while maintaining good mechanical strength and hydrogel conductivity. Finally, the mixed solution was then formed into flat-surface and hemispherical-surface hydrogel samples after being set for 24 hours. The resulting solution for the chitosan-derived/ graphene hydrogel is shown in Figure 3. Figure 4 shows the chitosan-derived/ graphene hydrogel produced on a flat surface and a hemispherical surface after settling for 24 hours. Ultrasonic cleaning with a frequency of 21.5-130 kHz was used to clean the hydrogel samples. The process began by placing the samples in a container filled with a cleaning solvent solution. After the cleaning cycle, the samples were rinsed with clean solvent and dried to remove any remaining impurities or solvent residues. This process ensured that the samples' surfaces were thoroughly cleaned, promoting better adhesion, improved surface properties, and enhanced performance in subsequent processing or application steps. Characterisation of the morphology of samples used an inverted microscope. In the evaporation experiment, a solar simulator lamp was used. A liquid-filled container undergoes three conditions: 1-hour and 12-hour continuous irradiation, and a control with no light exposure (see Figure 5). The testing condition was set up to mimic the effects of sunlight on the evaporation system, with varying irradiation durations. The testing parameters, including temperature and water mass/ volume, were recorded continuously to measure the evaporation rates. This experiment assessed the effect of sunlight on evaporation.

© 2026 The Authors. This work is licensed under a Creative Commons Attribution 4.0 International License

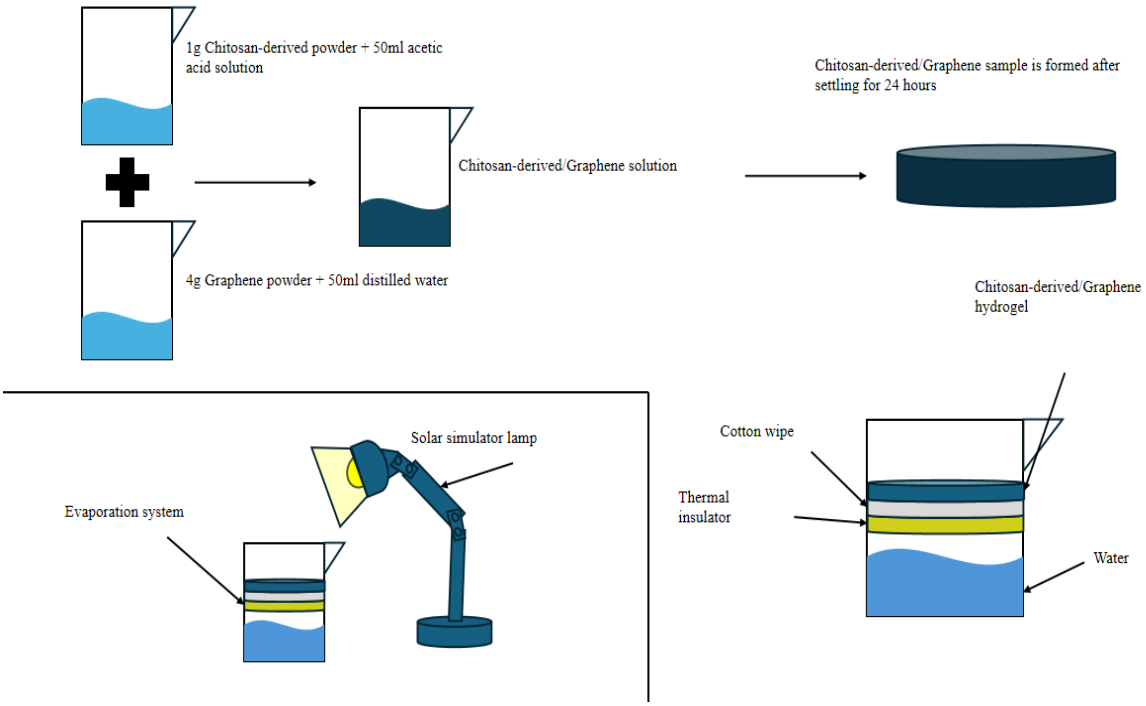


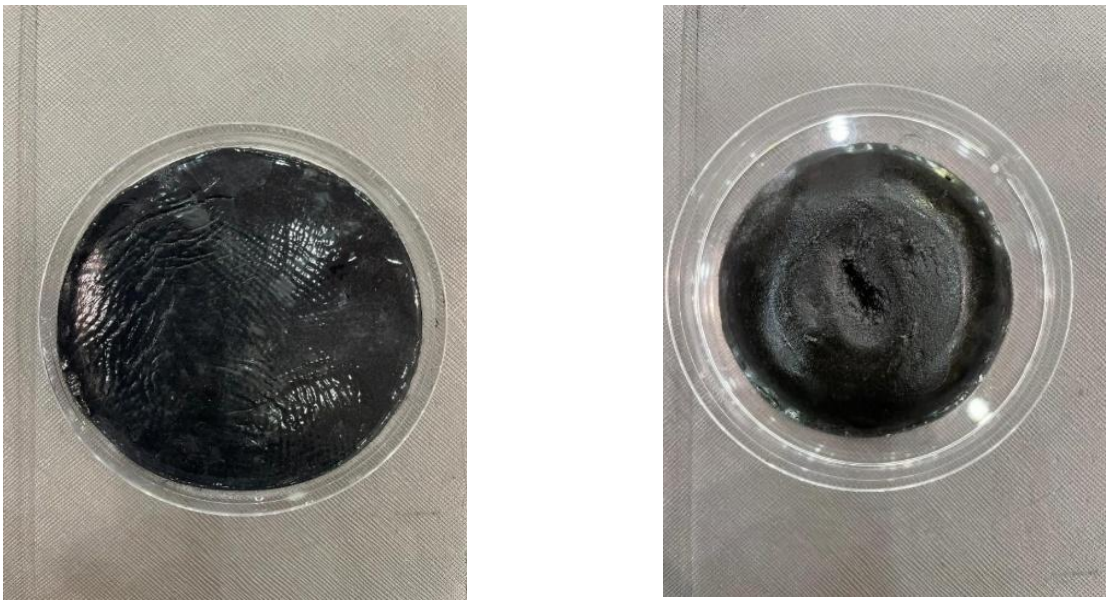
Figure 2. Fabrication process for producing chitosan-derived/graphene hydrogel.



(a) (b)

Figure 3. (a) Top view and (b) side view of the solution for chitosan-derived/ graphene hydrogel

© 2026 The Authors. This work is licensed under a Creative Commons Attribution 4.0 International License



(a) (b)

Figure 4. (a) Flat-surface hydrogel sample and (b) hemispherical-surface hydrogel sample

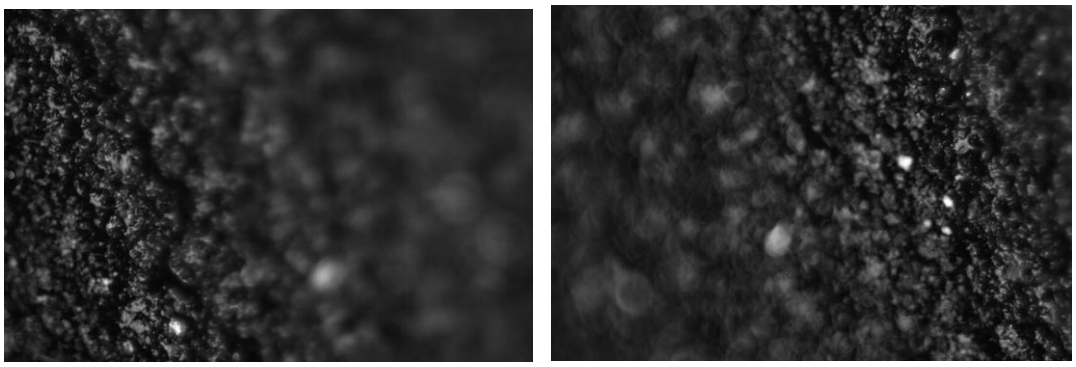


Figure 5. Evaporation experiment used a solar simulator lamp in three conditions 1-hour,12-hour continuous irradiation.

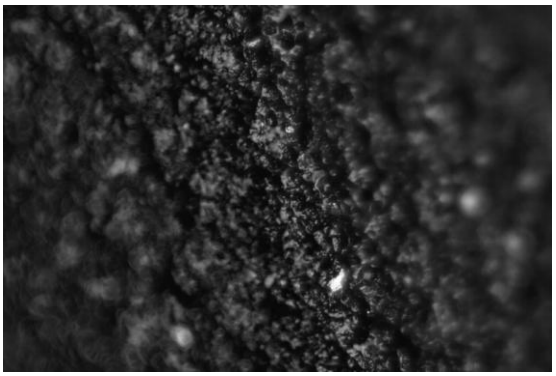
3. RESULTS AND DISCUSSION

Figure 6 (a) shows the moisture morphology of the hydrogel sample before irradiation. Figures 6 (b) and (c) show the ability of the flat-surface hydrogel samples to keep moisture after being irradiated for 1 hour and 12 hours. A similar moisture-retention trend after irradiation for 1 hour and 12 hours was observed in the hemispherical-surface hydrogel samples, as shown in Figure 7.

© 2026 The Authors. This work is licensed under a Creative Commons Attribution 4.0 International License

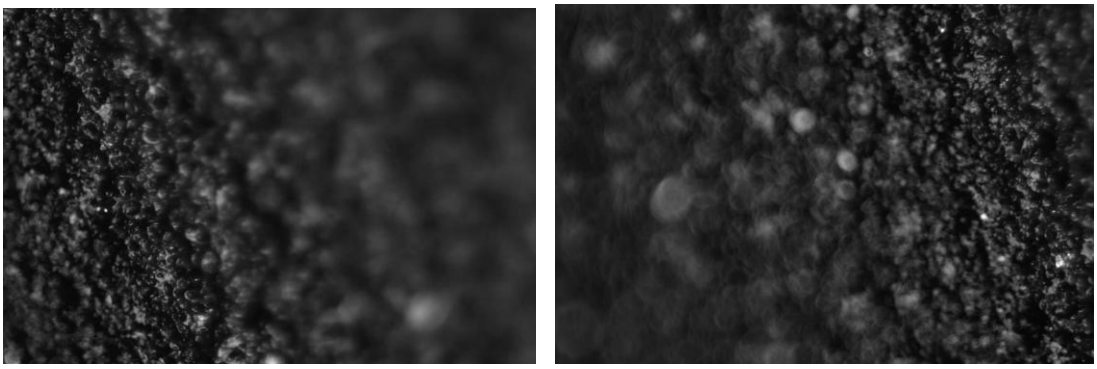


(a) (b)



(c)

Figure 6. Surface morphology of the flat-surface hydrogel samples



(a) (b)



(c)

Figure 7. Surface morphology of the hemispherical-surface hydrogel sample.

© 2026 The Authors. This work is licensed under a Creative Commons Attribution 4.0 International License

The temperature of both the flat-surface and hemispherical-surface hydrogel samples increased from 20 to 43 °C within the first 60 min, as shown in Figure 8. After about 200 min, the temperature reached stability. The maximum temperature of the flat-surface hydrogel sample is 57 °C, while the hemispherical-surface hydrogel sample exhibited a lower temperature distribution of 52 °C. The hydrogel's evaporation rate increases as the evaporator approaches a stable temperature, as does the evaporation efficiency. Once the temperature reaches equilibrium, the evaporation rate is also steady. In this case, the hemispherical-surface hydrogel sample showed a better ability to absorb heat more quickly and to retain heat at high temperatures. This change in evaporation rate from low to high temperatures is also reflected in the water-weight change curve in Figure 9. For the first 60 min of irradiation, heating was the dominant process, and evaporation stabilised after 720 min. It can be deduced that the hydrogel's evaporation space is adequately supplied with water as the evaporation surface area increases, thereby greatly improving evaporation performance [11], [12], [13], [14].

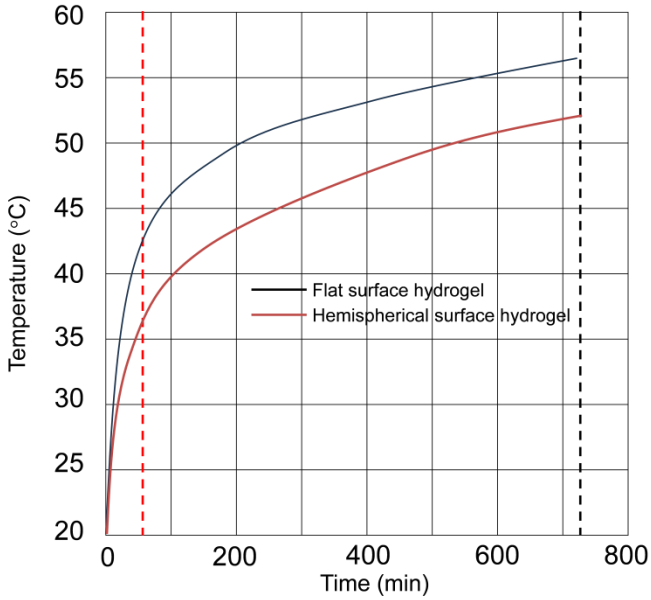


Figure 8. Temperature distribution of the flat-surface hydrogel and hemispherical-surface hydrogel samples under solar simulator irradiation for up to 12 hours.

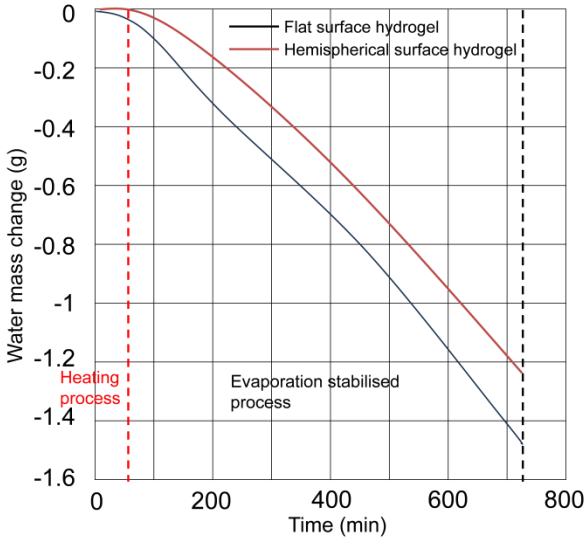


Figure 9. Water mass changes of the flat-surface hydrogel and the hemispherical-surface hydrogel samples under solar simulator irradiation for up to 12 hours.

The results presented in Figure 9 show that the initial water mass change of the flat-surface and hemispherical-surface hydrogel samples increased from 0 to −0.1 g over the first 60 min. After about 200 min, the water mass change reached stability. The maximum change in water mass for the flat-surface hydrogel sample is -

© 2026 The Authors. This work is licensed under a Creative Commons Attribution 4.0 International License

1.48 g. The mass loss for hemispherical-surface hydrogel samples was recorded as -1.22 g, which is lower than that of the flat-surface hydrogel sample. The evaporation rate of the flat-surface hydrogel and the hemispherical-surface hydrogel samples under solar simulator irradiation for up to 12 hours is shown in Figure 10. The hemispherical-surface hydrogel showed a higher evaporation rate of 0.09205 kgm^{-2} h^{-1}, which was higher than that of the flat-surface hydrogel sample of 0.04568 kgm^{-2} h^{-1}. This showed that the hemispherical-surface hydrogel is efficient at storing heat and serving as an evaporative system. The calculation of the evaporation rate and the surface area of the flat-surface and hemispherical-surface hydrogel samples under solar simulator irradiation for up to 12 hours is shown in Table 1.

Table 1. The calculation of the evaporation rate and the surface area of the (a) flat-surface and (b) hemispherical-surface hydrogel samples under solar simulator irradiation for up to 12 hours.

Parameter	**Flat-surface hydrogel**	**Hemispherical-surface hydrogel**
Radius, r	3.75 cm	3.75 cm
Height, h	10 cm	-
Surface area equation	$2\pi rh + 2\pi r^2$	$3\pi r^2$
Surface area calculation	$2\pi(3.75)(10) + 2\pi(3.75)^2$	$3\pi(3.75)^2$
Surface area	323.98 cm^2	132.54 cm^2
Surface area	0.032398 m^2	0.013254 m^2
Total water mass loss	1.48 g	1.22 g
Water mass conversion	0.00148 kg	0.00122 kg
Evaporation rate equation	Total water mass loss / Surface area	Total water mass loss / Surface area
Calculation	0.00148 / 0.032398	0.00122 / 0.013254
Evaporation rate	0.045682 kg m^{-2} h^{-1}	0.092048 kg m^{-2} h^{-1}

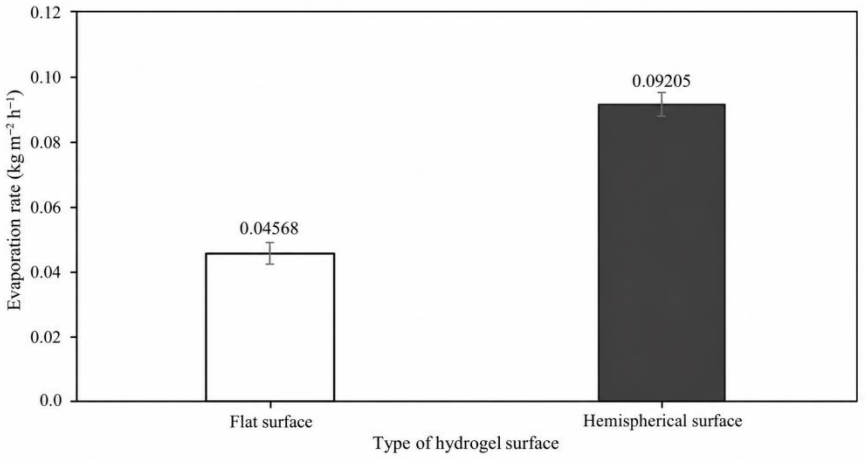


Figure 10. Evaporation rate of the flat-surface hydrogel and the hemispherical-surface hydrogel samples under solar simulator irradiation for up to 12 hours.

Figure 11 compares the temperature distributions of various hydrogel types reported in previous studies. The chitosan hydrogel exhibits the highest temperature distribution efficiency, likely due to its water-retentive structure, followed by carbon nanoparticles and graphene [11], [12], [15]. A combination of chitosan-derived and graphene hydrogels outperforms other hydrogels. Results showed that the production of new chitosan-derived, graphene hydrogels exhibits promising evaporation efficiency and thermal distribution, despite each hydrogel having its own unique strengths. The comparison of water mass changes of various hydrogels is shown in Figure 12. The largest change in water mass was observed in chitosan hydrogel, followed by carbon nanoparticles and graphene. The chitosan-derived, graphene hydrogel exhibited the smallest change in water mass, indicating rapid heat absorption and making it highly effective for solar evaporation. The results indicate that a lower temperature distribution in the

© 2026 The Authors. This work is licensed under a Creative Commons Attribution 4.0 International License

hemispherical-surface hydrogel can still yield a higher evaporation rate due to several factors, i.e., a small surface area exposed to air and the ability to retain moisture after 12 hours of irradiation.

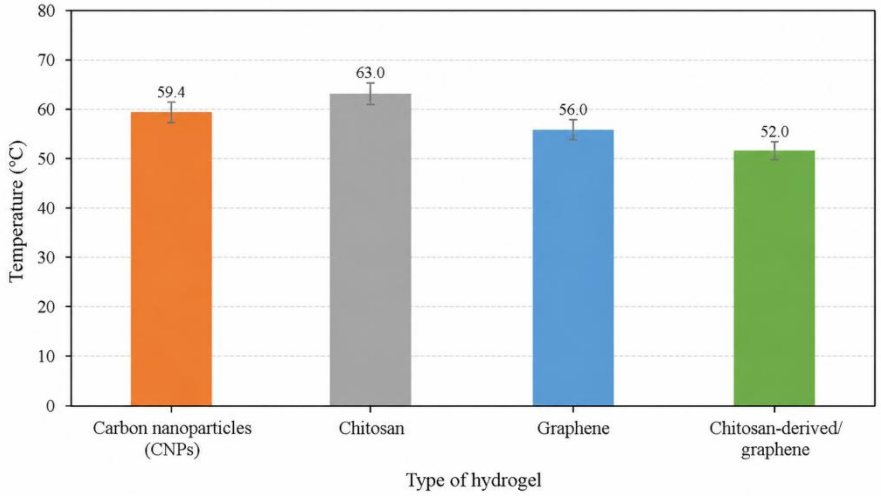


Figure 11. Comparison of the temperature distribution of various types of hydrogels based on previous studies.

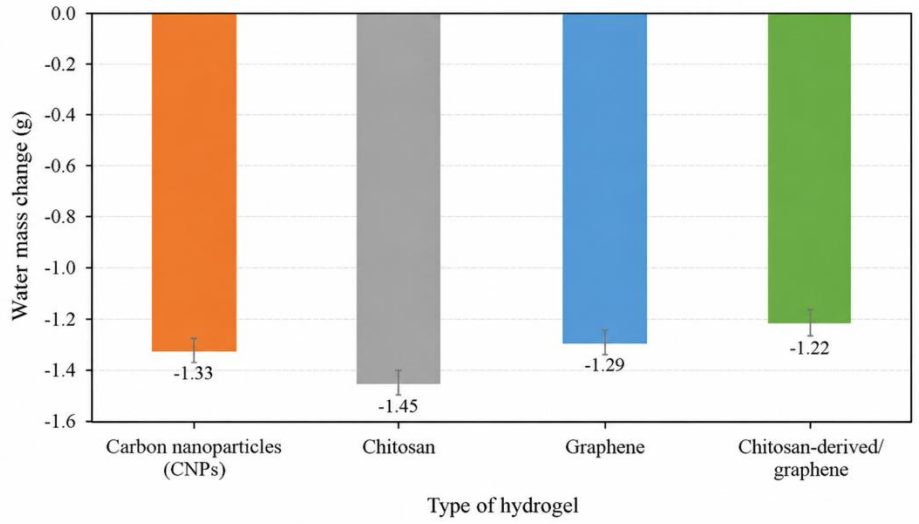


Figure 12. Comparison of the water mass change of various types of hydrogels based on previous studies.

4. CONCLUSION

The chitosan-derived/graphene hydrogel was successfully fabricated in two types, i.e., flat and hemispherical surfaces. The results showed that the hemispherical-surface hydrogel exhibited promising performance for solar evaporation compared to the flat-surface hydrogels. The hemispherical-surface hydrogels have a lower temperature distribution and water mass loss of 52 °C and -1.22 g, respectively, compared to the flat-surface hydrogels. This has resulted in a higher evaporation rate of 0.09205 kgm^{-2} h^{-1} than that of the flat-surface hydrogel, 0.04568 kgm^{-2} h^{-1}, which could be attributed to the small surface area of the hemispherical-surface hydrogel exposed to air.

ACKNOWLEDGEMENTS

The authors gratefully acknowledge the Ministry of Higher Education, Malaysia, and the Department of Polytechnic and Community College Education for their financial support and facilities, which were instrumental in completing this study.

AUTHORS' CONTRIBUTIONS

H.P.L. and **L.C.** contributed to the conceptualization of the study, methodology development, supervision, formal analysis, data validation, as well as writing the original draft and reviewing the manuscript. **L.C.** and **I.R.A.** were responsible for investigation, data curation, formal analysis, data visualization, and preparation of the original draft. Meanwhile, **H.P.L**. and **I.R.A.** contributed to conceptualization, methodology development, project supervision, project administration, and manuscript review and editing.

© 2026 The Authors. This work is licensed under a Creative Commons Attribution 4.0 International License

REFERENCES

[1] C. Thambiliyagodage, M. Jayanetti, A. Mendis, G. Ekanayake, H. Liyanaarachchi, and S. Vigneswaran, "Recent advances in chitosan-based applications—A review," Materials, vol. 16, no. 5, Art. no. 2073, Mar. 2023, doi: 10.3390/ma16052073.

[2] M. Nasrollahzadeh, M. Sajjadi, S. Iravani, and R. S. Varma, "Starch, cellulose, pectin, gum, alginate, chitin and chitosan derived (nano)materials for sustainable water treatment: A review," Carbohydr. Polym., vol. 251, Art. no. 116986, Jan. 2021, doi: 10.1016/j.carbpol.2020.116986.

[3] Z. Feng, K. Odelius, and M. Hakkarainen, "Tunable chitosan hydrogels for adsorption: Property control by biobased modifiers," Carbohydr. Polym., vol. 196, pp. 135–145, Sep. 2018, doi: 10.1016/j.carbpol.2018.05.029.

[4] A. Narayanan, R. Kartik, E. Sangeetha, and R. Dhamodharan, "Super water absorbing polymeric gel from chitosan, citric acid and urea: Synthesis and mechanism of water absorption," Carbohydr. Polym., vol. 191, pp. 152–160, Jul. 2018, doi: 10.1016/j.carbpol.2018.03.028.

[5] Z. Feng, M. Hakkarainen, H. Grützmacher, A. Chiappone, and M. Sangermano, "Photocrosslinked chitosan hydrogels reinforced with chitosan-derived nano-graphene oxide," Macromol. Chem. Phys., vol. 220, no. 13, Art. no. 1900174, 2019, doi: 10.1002/macp.201900174.

[6] Y. H. Wang et al., "Evaluation of chitosan-based dressings in a swine model of artery-injury-related shock," Sci. Rep., vol. 9, no. 1, Art. no. 14608, 2019, doi: 10.1038/s41598-019-51208-7.

[7] Y. Xu, K. Sheng, C. Li, and G. Shi, "Self-assembled graphene hydrogel via a one-step hydrothermal process," ACS Nano, vol. 4, no. 7, pp. 4324–4330, Jul. 2010, doi: 10.1021/nn101187z.

[8] K. X. Sheng, Y. X. Xu, C. Li, and G. Q. Shi, "High-performance self-assembled graphene hydrogels prepared by chemical reduction of graphene oxide," New Carbon Mater., vol. 26, no. 1, pp. 9–15, 2011, doi: 10.1016/S1872-5805(11)60062-0.

[9] H. N. Lim, N. M. Huang, S. S. Lim, I. Harrison, and C. H. Chia, "Fabrication and characterization of graphene hydrogel via hydrothermal approach as a scaffold for preliminary study of cell growth," Int. J. Nanomedicine, vol. 6, pp. 1817–1823, 2011, doi: 10.2147/IJN.S23392.

[10] G. Sun, B. Li, J. Ran, X. Shen, and H. Tong, "Three-dimensional hierarchical porous carbon/graphene composites derived from graphene oxide-chitosan hydrogels for high performance supercapacitors," Electrochim. Acta, vol. 171, pp. 13–22, Jul. 2015, doi: 10.1016/j.electacta.2015.05.009.

[11] M. Zhu, X. Liu, Y. Tian, A. Caratenuto, F. Chen, and Y. Zheng, "Dome-arrayed chitosan/PVA hydrogel-based solar evaporator for steam generation," Sci. Rep., vol. 12, no. 1, Art. no. 4403, Mar. 2022, doi: 10.1038/s41598-022-08589-z.

[12] Z. Li et al., "Chitosan-derived carbon aerogel modified with lignin carbon quantum dots for efficient solar evaporation," Chem. Eng. J., vol. 486, Art. no. 150157, Apr. 2024, doi: 10.1016/j.cej.2024.150157.

[13] W. M. J. Karen, Z. Wang, W. Y. H. Liew, and G. J. H. Melvin, "Low-cost and sustainable carbonized sawdust based solar absorber for solar vapor generation towards seawater desalination," Waste Biomass Valorization, vol. 14, no. 9, pp. 3071–3080, Sep. 2023, doi: 10.1007/s12649-023-02067-x.

[14] W. M. J. Karen, C. Y. Wong, and G. J. H. Melvin, "Desalination of seawater using carbon-coated solar absorber in solar still," IOP Conf. Ser. Mater. Sci. Eng., vol. 1217, no. 1, Art. no. 012001, 2022, doi: 10.1088/1757-899X/1217/1/012001.

[15] F. Wang et al., "Chitosan/reduced graphene oxide-modified spacer fabric as a salt-resistant solar absorber for efficient solar steam generation," J. Mater. Chem. A, vol. 7, no. 31, pp. 18311–18317, 2019, doi: 10.1039/C9TA05859A.

© 2026 The Authors. This work is licensed under a Creative Commons Attribution 4.0 International License